DOI: 10.1002/ejic.201100061

Orthomolybdates in the Cs–$Fe^{II,III}$–Mo–O System: $Cs_4Fe(MoO_4)_3$, $Cs_2Fe_2(MoO_4)_3$ and $CsFe_5(MoO_4)_7$

Touyana Namsaraeva,[a] Bair Bazarov,[a] Daria Mikhailova,*[b,c] Natalia Kuratieva,[c,d] Angelina Sarapulova,[b] Anatoliy Senyshyn,[c] and Helmut Ehrenberg[b]

Keywords: Iron / Molybdenum / Magnetic properties / Multi-k structure / X-ray diffraction

Three new complex molybdenum oxides – $Cs_2Fe_2(MoO_4)_3$, $Cs_4Fe(MoO_4)_3$ and $CsFe_5(MoO_4)_7$ – with average oxidation states of Fe +2 and +2.6 were obtained during a study of phase formation in the system Cs–$Fe^{II,III}$–Mo–O and investigated by X-ray single-crystal analysis at room temperature and 100 K. The structure of cubic $Cs_2Fe_2(MoO_4)_3$ [$P2_13$, a = 10.9161(2) Å, Z = 4] is very similar to the one of pseudocubic $Cs_2Co_2(MoO_4)_3$ with a weak orthorhombic distortion. Hexagonal $Cs_4Fe(MoO_4)_3$ [$P\bar{6}2c$, a = 6.2922(16) Å, c = 23.937(13) Å, Z = 2] is isostructural to the high-temperature modification of $Rb_4Mn(MoO_4)_3$. $CsFe_5(MoO_4)_7$ crystallizes in monoclinic symmetry [$P2_1/m$, a = 6.9239(6) Å, b = 21.4477(19) Å, c = 8.6374(8) Å, β = 101.667(2)°, Z = 2] and represents a new structure type. This structure contains three crystallographically independent Fe sites and consists of isolated FeO_6 octahedra and Fe_4O_{18} units of edge-sharing FeO_6 octahedra, which are connected with MoO_4 tetrahedra through corners, thus forming a three-dimensional framework. $CsFe_5(MoO_4)_7$ orders magnetically with a ferromagnetic component at T_C = 10 K, proposed as a canted antiferromagnet. Its antiferromagnetic structure at 0 T was described by combination of two propagation vectors **k** = (1/2, 0, 0) and **k** = (0, 0, 0) with magnetic moments of 2.6, 1.6 and 3.5 μ_B for three independent Fe sites. Two magnetic-field-induced transitions are observed at 0.25 and 1.9 T at 2 K.

Introduction

Complex orthomolybdates with alkaline and 3d elements crystallize often in similar compositions but quite different structure types, which are determined by the sizes of the alkaline elements. For example, the stoichiometry $A_2M_2(MoO_4)_3$ is known for all alkaline elements A from Li to Cs and also for Tl and Ag. Smaller cations Li and Na form an orthorhombic sodium superionic conductor (NaSICON)-type structure with channels along the a axes, which are half-filled by alkaline cations. This structure type was first described for $NaCo_{2.31}(MoO_4)_3$[1] and is known for A = Li in combination with all 3d elements.[2–4] Due to the rather weak bonding of the alkaline ions, high ionic conductivity is often observed for these compounds at elevated temperature. These molybdates might also be considered as intercalation materials, because the channels are only partially occupied and can host additional alkaline ions such as Li^+ or Na^+, which can be inserted into the structure by a chemical or electrochemical route. $K_2M_2(MoO_4)_3$ with 3d elements as M^{2+} crystallize in the $K_2Zn_2(MoO_4)_3$ structure type[5] with M_4O_{18} tetramers of edge-sharing MO_6 octahedra and K atoms that occupy large spaces in the structure. The low density of these structures could lead to pressure-induced phase transitions with the formation of more dense polymorphs, which was investigated and confirmed for $K_2Co_2(MoO_4)_3$.[6] Rb-containing orthomolybdates adopt either the $K_2Zn_2(MoO_4)_3$ structure type for M = Ni, Cu, Zn or the langbeinite $K_2Mg_2(SO_4)_3$ type[2] with isolated MO_6 octahedra. $Cs_2M_2(MoO_4)_3$ compositions are only known with $K_2Mg_2(SO_4)_3$-like structures.[2]

The possibility of Fe to adopt different oxidation states between +2 and +3 in the same orthomolybdate gives an additional degree of freedom for phase composition and crystal structure formation. For example, four orthomolybdate phases with three-dimensional networks of MoO_4 tetrahedra and FeO_6 octahedra and different connectivity schemes are reported for the $Na_xFe_y(MoO_4)_z$ system that have not been found for other 3d cations: $NaFe_4(MoO_4)_5$, α-$NaFe_2(MoO_4)_3$, β-$NaFe_2(MoO_4)_3$ and $Na_3Fe_2(MoO_4)_3$.[7] For the latter one, the unusual combination of oxidation states Fe^{III}/Mo^{V} was postulated. In the Ag–$Fe^{II,III}$–Mo–O system, $AgFe_2(MoO_4)_3$ was found isostructural to α-$NaFe_2(MoO_4)_3$.[8] For the Cs–Fe–Mo–O system, only the compounds $CsFe(MoO_4)_2$, $Cs_5Fe(MoO_4)_4$ and $Cs_3FeMo_4O_{15}$ with Fe^{III} have been described so far.[2,9,10]

[a] Baikal Institute of Nature Management, Siberian Branch, Russian Academy of Sciences,
Sakh'yanova Street 6, Ulan-Ude, Russia
[b] IFW Dresden, Institute for Complex Materials,
Helmholtzstrasse 20, 01069 Dresden, Germany
[c] Institute for Materials Science, Technische Universität Darmstadt,
Petersenstrasse 23, 64287 Darmstadt, Germany
[d] Nikolaev Institute of Inorganic Chemistry, Siberian Branch, Russian Academy of Sciences,
prosp. Lavrentieva 3, Novosibirsk 630090, Russia

The aim of the present work was the preparation of new Cs–Fe^{II,III}–Mo–O compounds under reducing conditions, their structural characterization and the comparison with known structure types.

Results

Composition and Crystal Structures of Cs,Fe Molybdates

During the investigation of the Cs–Fe^{II,III}–Mo–O system in addition to the already known phase $CsFe(MoO_4)_2$[9] three new compounds were identified: $Cs_2Fe_2(MoO_4)_3$ and $Cs_4Fe(MoO_4)_3$ with Fe^{+2} and $CsFe_5(MoO_4)_7$ with the average oxidation state +2.6 for Fe. All obtained phases represent orthooxomolybdates, because no direct links between MoO_4 tetrahedra exist in the structures, and all oxygen atoms belong to exactly one MoO_4 tetrahedron. Single-crystal X-ray diffraction experiments at room temperature and 100 K revealed no phase transition in this temperature range.

Crystal Structure of $Cs_2Fe_2(MoO_4)_3$

The crystal structure (Figure 1) of cubic $Cs_2Fe_2(MoO_4)_3$ ($P2_13$) is very similar to the one of pseudocubic langbeinite-like $Cs_2Co_2(MoO_4)_3$ ($P2_12_12_1$). The latter, however, shows a weak orthorhombic distortion.[11] The structure represents a framework of corner-sharing MoO_4 tetrahedra and FeO_6 octahedra with large ellipsoidal cavities, in which two crystallographically independent Cs atoms with different average Cs–O distances are situated. Atomic coordinates and equivalent isotropic displacements are listed in Table 1. The coordination surrounding Cs(1) atoms consists of three FeO_6 octahedra and six MoO_4 tetrahedra, so that almost closed $Fe_4Mo_6O_{36}$ units (Figure 2) can be defined, whereas Cs(2) atoms are surrounded by $Fe_7Mo_6O_{48}$ units (Figure 3). $Fe_4Mo_6O_{36}$ and $Fe_7Mo_6O_{48}$ units form together a larger $Fe_8Mo_9O_{60}$ cavity with two caesium atoms inside. The slight orthorhombic distortion in the $Cs_2Co_2(MoO_4)_3$ structure was deduced in the literature[11] from much better temperature parameters and R factors compared with the cubic structure and corresponds to small displacements of some Mo and O atoms from their positions so that three crystallographically independent Mo atoms and twelve O atoms appeared. According to the group/subgroup relations, $P2_12_12_1$ is a subgroup of $P2_13$, so that a possible phase transformation in $Cs_2Co_2(MoO_4)_3$ from $P2_12_12_1$ into $P2_13$ was proposed in the literature[11] at higher temperature. Our attempts to refine the crystal structure of $Cs_2Fe_2(MoO_4)_3$ with $P2_12_12_1$ symmetry did not give significantly better R indices so that the cubic structure model was preferred.

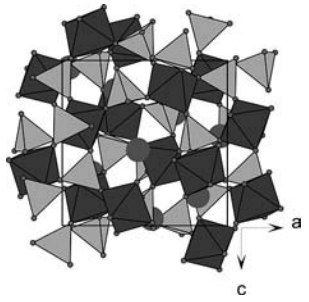

Figure 1. Crystal structure of $Cs_2Fe_2(MoO_4)_3$, viewed along one crystallographic axis, with FeO_6 octahedra, MoO_4 tetrahedra, and Cs as spheres.

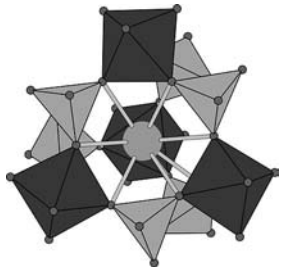

Figure 2. CsO_8 polyhedron in $Cs_2Fe_2(MoO_4)_3$, which forms partially closed $Fe_4Mo_6O_{36}$ units.

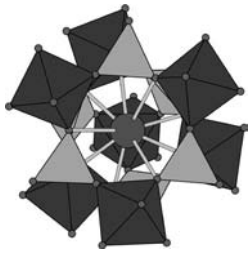

Figure 3. CsO_9 polyhedron in $Cs_2Fe_2(MoO_4)_3$, which forms partially closed $Fe_7Mo_6O_{48}$ units.

Table 1. Atomic coordinates and equivalent isotropic displacement parameters [$Å^2 \times 10^3$] for $Cs_2Fe_2(MoO_4)_3$ ($P2_13$).

Atom type	Wyckoff positions	x	y	z	Occupancy	U_{eq}[a]
Cs(1)	4*a*	0.179380(14)	0.320620(14)	0.679380(14)	1	0.02046(6)
Cs(2)	4*a*	0.457613(17)	0.957613(17)	0.542387(17)	1	0.02955(8)
Mo(1)	12*b*	0.300614(17)	0.623626(17)	0.525973(17)	1	0.01052(5)
Fe(1)	4*a*	0.33737(3)	0.33737(3)	0.33737(3)	1	0.01066(11)
Fe(2)	4*a*	0.61246(3)	0.61246(3)	0.61246(3)	1	0.01152(11)
O(1)	12*b*	0.27587(18)	0.48544(17)	0.44750(17)	1	0.0249(4)
O(2)	12*b*	0.45432(16)	0.67110(17)	0.51709(18)	1	0.0242(4)
O(3)	12*b*	0.25187(18)	0.60297(17)	0.67761(16)	1	0.0226(4)
O(4)	12*b*	0.21150(17)	0.73545(18)	0.45198(18)	1	0.0253(4)

[a] U_{eq} is defined as one-third of the trace of the orthogonalized U_{ij} tensor.

From the structural point of view, paramagnetic behaviour with only weak magnetic interactions is expected for $Cs_2Fe_2(MoO_4)_3$ due to a diluted character of Fe distribution in the structure and a relatively long Fe–Fe distance (5.20 Å) between nearest neighbours.

Crystal Structure of $CsFe_5(MoO_4)_7$

A monoclinic unit cell with a = 6.9239(6) Å, b = 21.4477(19) Å, c = 8.6374(8) Å and β = 101.667(2)° was determined by X-ray single-crystal diffraction for crystals synthesized at 1023 K and slowly cooled in the furnace. The structure was solved and refined in the space group $P2_1/m$ (Table 2), thus giving the composition $CsFe_5(MoO_4)_7$ (see Figure 4). Since no entries that concern compounds with analogous cell parameters or $AB_5C_7X_{28}$ composition were found in the Inorganic Crystal Structure Database (ICSD),[12] a new crystal-structure type, namely, the $CsFe_5(MoO_4)_7$ type, was established. It consists of separate FeO_6 octahedra with an average Fe–O distance of 2.04(2) Å, and zigzag Fe_4O_{18} units of edge-sharing FeO_6 octahedra with an average Fe–O distance of 2.04(6) Å (see Figure 5), which are connected through corners with MoO_4 tetrahedra [average Mo–O distance is 1.76(4) Å]. There is no direct contact between MoO_4 units. The existence of tetramers Fe_4O_{18} in $CsFe_5(MoO_4)_7$ resembles structural fragments of the $K_2Zn_2(MoO_4)_3$ structure type[5] (see Figure 5). Due to a smaller amount of MoO_4 groups per 3d cation in $K_2Zn_2(MoO_4)_3$ more MoO_4 tetrahedra are connected with ZnO_6 through two oxygen atoms, whereas in $CsFe_5(MoO_4)_7$ more MoO_4 tetrahedra have terminated oxygen atoms.

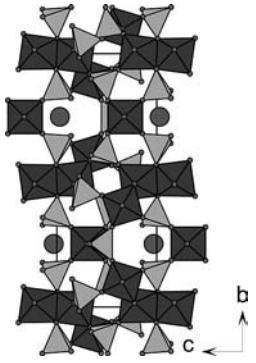

Figure 4. Crystal structure of $CsFe_5(MoO_4)_7$ viewed along the a axis.

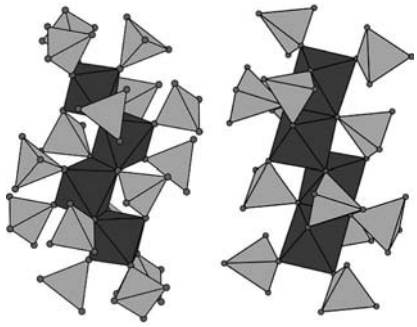

Figure 5. Fe_4O_{18} units of edge-sharing FeO_6 octahedra in $CsFe_5(MoO_4)_7$ (left) and Zn_4O_{18} units of edge-sharing ZnO_6 octahedra in $K_2Zn_2(MoO_4)_3$[5] (right).

Caesium atoms occupy channels in the structure along the a axis (Figures 4 and 6). Atomic coordinates and equivalent isotropic displacements are listed in Table 2. From a structural point of view, high ionic conductivity of Cs ions at elevated temperature may be expected for this phase.

Table 2. Atomic coordinates and equivalent isotropic displacement parameters [$Å^2 \times 10^3$] for $CsFe_5(MoO_4)_7$ ($P2_1/m$).

Atom type	Wyckoff positions	x	y	z	Occupancy	U_{eq}
Cs(1)	2e	0.50338(4)	0.2500	0.03046(4)	1	0.02452(7)
Fe(1)	4f	0.35239(5)	0.099757(19)	0.34087(5)	1	0.00996(8)
Fe(2)	2e	0.95405(8)	0.2500	0.68836(7)	1	0.00921(11)
Fe(3)	4f	0.02621(6)	0.502639(18)	0.18821(5)	1	0.01014(8)
Mo(1)	4f	0.01243(3)	0.142087(11)	0.03242(3)	1	0.01209(6)
O(11)	4f	0.2613(3)	0.14571(10)	0.1401(3)	1	0.0173(4)
O(12)	4f	–0.0021(4)	0.18389(11)	–0.1436(3)	1	0.0270(5)
O(13)	4f	–0.0428(3)	0.06018(9)	–0.0058(2)	1	0.0142(4)
O(14)	4f	–0.1389(3)	0.17534(12)	0.1425(3)	1	0.0274(5)
Mo(2)	4f	0.88086(3)	0.107538(11)	0.44898(3)	1	0.00993(6)
O(21)	4f	0.6373(3)	0.09861(11)	0.3444(3)	1	0.0208(5)
O(22)	4f	0.9261(3)	0.18403(10)	0.5123(3)	1	0.0179(4)
O(23)	4f	0.9083(3)	0.06171(11)	0.6181(3)	1	0.0218(5)
O(24)	4f	1.0554(3)	0.07873(9)	0.3321(2)	1	0.0138(4)
Mo(3)	2e	0.41472(5)	0.2500	0.56331(4)	1	0.01068(7)
O(31)	2e	0.6561(4)	0.2500	0.6740(4)	1	0.0211(7)
O(32)	2e	0.2530(4)	0.2500	0.6957(4)	1	0.0187(6)
O(33)	4f	0.3721(3)	0.31728(11)	0.4445(3)	1	0.0262(5)
Mo(4)	4f	0.52933(3)	0.542663(11)	0.24695(3)	1	0.01060(6)
O(41)	4f	0.3294(3)	0.48420(9)	0.2230(2)	1	0.0121(4)
O(42)	4f	0.7367(3)	0.51692(11)	0.1761(3)	1	0.0230(5)
O(43)	4f	0.4430(4)	0.60967(11)	0.1525(3)	1	0.0292(6)
O(44)	4f	0.6050(3)	0.55925(12)	0.4498(3)	1	0.0227(5)

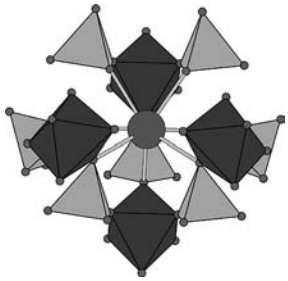

Figure 6. CsO_{10} polyhedron in $CsFe_5(MoO_4)_7$.

Crystal Structure of $Cs_4Fe(MoO_4)_3$

The structure of $Cs_4Fe(MoO_4)_3$ was solved in the space group $P\bar{6}2c$. There are two crystallographically independent molybdenum atoms in the structure with a tetrahedral coordination of oxygen atoms.

The coordination tetrahedron around Mo(2) can be described as consisting of a trigonal basis formed by three oxygen atoms O(3), which lies parallel to the *ab* plane. The positions of the central Mo(2) and the fourth O(4) (both on 4*f* sites) are split (Table 3). The Mo atoms statistically occupy one of these positions in different unit cells. The position of the fourth oxygen atom, O(4), depends on which Mo split position is occupied, above or below the basis plane.

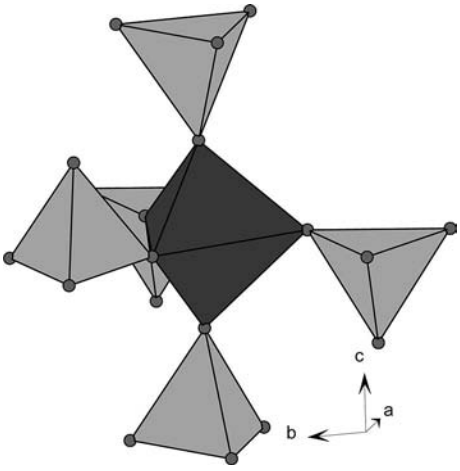

Figure 7. Trigonal-bipyramidal coordination of Fe in $Cs_4Fe(MoO_4)_3$.

The Fe atoms have unusual trigonal-bipyramidal coordination (see Figure 7) with $d(Fe–O)_{equat.}$ = 2.156(6) Å and $d(Fe–O)_{apic.}$ = 1.958(4) Å. MoO_4 tetrahedra and FeO_5 bipyramids form layers perpendicular to the *c* axis (Figures 8 and 9), and caesium atoms occupy free spaces along the *c*

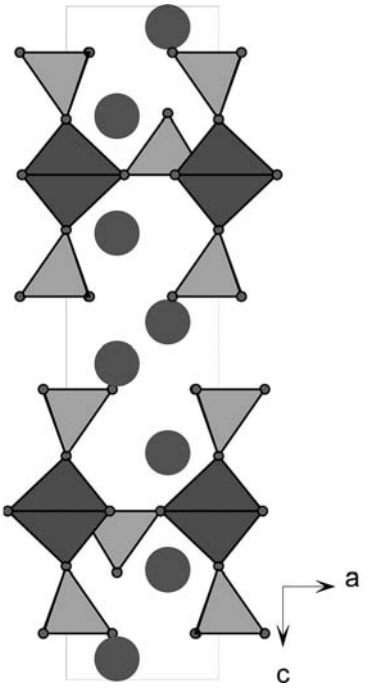

Figure 8. Structure of $Cs_4Fe(MoO_4)_3$ viewed along the *b* axis.

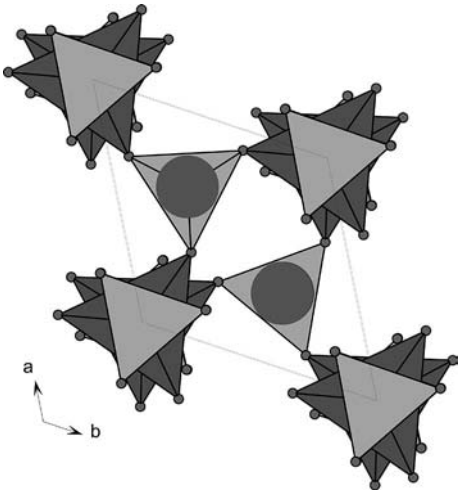

Figure 9. Structure of $Cs_4Fe(MoO_4)_3$ viewed along the *c* axis.

Table 3. Atomic coordinates and equivalent isotropic displacement parameters [Å$^2 \times 10^3$] for $Cs_4Fe(MoO_4)_3$ ($P\bar{6}2c$).

Atom type	Wyckoff positions	*x*	*y*	*z*	Occupancy	U_{eq}
Cs(1)	4*f*	0.6667	0.3333	0.030963(13)	1	0.02262(10)
Cs(2)	4*f*	0.3333	0.6667	0.163170(14)	1	0.02978(11)
Mo(1)	4*e*	0.0000	0.0000	0.093646(15)	1	0.01691(10)
Mo(2)	4*f*	0.6667	0.3333	0.23098(4)	0.5	0.01997(19)
Fe(1)	2*b*	0.0000	0.0000	0.2500	1	0.0227(2)
O(1)	4*e*	0.0000	0.0000	0.16820(16)	1	0.0457(12)
O(2)	12*i*	0.1471(15)	0.3011(4)	0.06888(9)	1	0.0311(6)
O(3)	6*h*	0.3793(10)	0.2869(11)	0.2500	1	0.0482(15)
O(4)	4*f*	0.6667	0.3333	0.1591(4)	0.5	0.044(3)

axis. This model with a disorder of some Mo and O ions is in good agreement with an earlier report on isostructural $Rb_4Mn(MoO_4)_3$.[13] Note that the loose crystal structure of $Cs_4Fe(MoO_4)_3$ could provide fast degradation in contact with moisture. Actually, $Cs_4Fe(MoO_4)_3$ samples contained water after storage in air for several hours.

Synthesis of Polycrystalline $CsFe_5(MoO_4)_7$ and Magnetization Studies

A nearly phase-pure polycrystalline sample of $CsFe_5(MoO_4)_7$ was obtained, according to X-ray powder diffraction (see Figure 10), by synthesis in dynamic vacuum with a steplike temperature increase up to a final temperature of 973 K over 20 h. Less than 2% (w/w) monoclinic α-$FeMoO_4$ (space group *C*2/*m*) was detected as an admixture, which is antiferromagnetic below 35 K.[14] The temperature dependencies of magnetization (Figure 11a) of $CsFe_5(MoO_4)_7$ show a difference between zero-field-cooled (ZFC) and field-cooled (FC) measurements below 10 K, which is attributed to the onset of a ferro- or ferrimagnetic ordering. α-$FeMoO_4$ does not contribute to these observed magnetic properties of $CsFe_5(MoO_4)_7$. At higher temperatures, the magnetization obeys a modified Curie–Weiss law $M(T) = C/(T - \theta) + M_0$ with $\theta = -17.3(9)$ K, and a least-squares fit to the FC data between 30 and 350 K is shown in the inset of Figure 11a. Note that the spontaneous magnetization in zero-field has a random orientation with respect to the later applied magnetic field, so that the negative magnetizations at low temperatures are not unusual. The change to positive magnetizations at about 7 K reflects the temperature dependence of the coercivity field $H_C(T)$, which reaches the external applied field strength of 100 G at this temperature. A paramagnetic moment of 5.20(1) μ_B per Fe ion is calculated from the Curie constant *C* as an average value from FC and ZFC data. Magnetic hysteresis loops at 2 K (Figure 11b) show two stepwise increases in magnetization with increasing field. The corresponding magnetization values at zero field are obtained from an extrapolation of fits in the linear region and are 20.84, 7.33 and 0.98 emu g^{-1}, which is equivalent to 5.72 μ_B per formula unit (f.u.), 2.01 and 0.27 μ_B per f.u., respectively. In light of five Fe atoms per f.u. on three distinct sites, the low-field region is most probably a canted antiferromagnet. The weak ferromagnetic component results from a small canting angle, whereas the dominant component is antiferromagnetic in agreement with the negative Curie–Weiss temperature, θ. The intermediate-field magnetic structure is probably a spin-flop phase with an increased canting angle in the field direction. The high-field magnetic structure could already represent a field-induced spin-flip phase, but with only the Fe(2) sublattice with isolated FeO_6 octahedra on the 2e site aligned in the field direction. A spin flip on the 4*f* sites of Fe(1) or Fe(3), which form tetramers of edge-sharing FeO_6 octahedra, would contribute to the magnetization by about 8 or 10 μ_B per f.u. for each of these two sites for spin-only magnetism, depending on the corresponding Fe^{2+} or Fe^{3+} states. In contrast, the high-field magnetization behaviour up to 6 T is far from expected saturation at about 23 μ_B per f.u.,

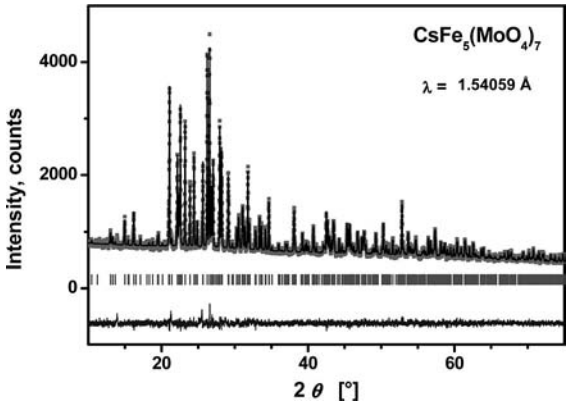

Figure 10. Powder diffraction pattern of $CsFe_5(MoO_4)_7$ with observed and fitted profiles together with the corresponding difference curve (Cu-$K_{\alpha 1}$). One reflection at 14.8° corresponds to α-$FeMoO_4$ (less than 2% w/w) with a = 9.808(1) Å, b = 8.960(1) Å, c = 7.657(1) Å, β = 114.03(1)°, space group *C*2/*m*.[14]

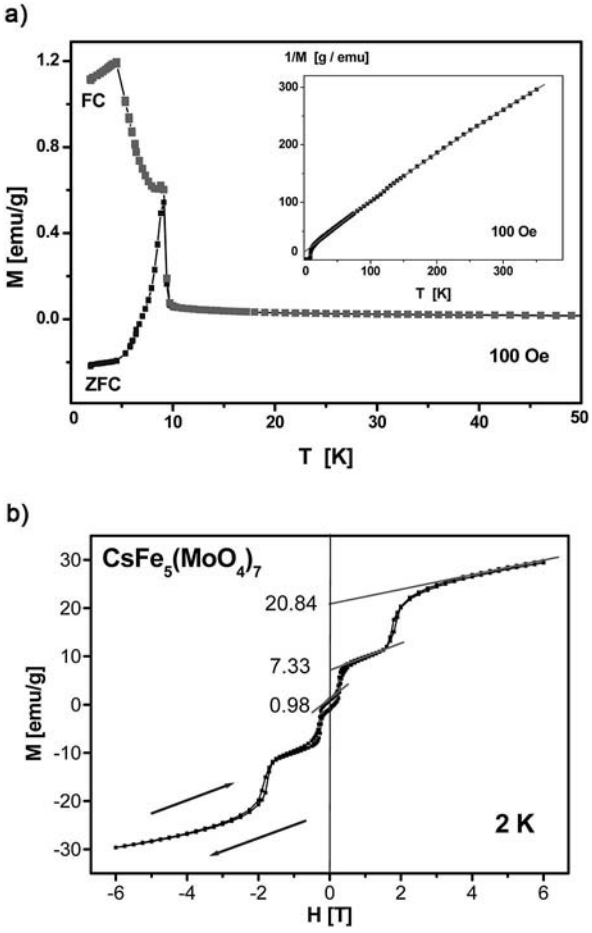

Figure 11. (a) Temperature dependence of magnetization of $CsFe_5(MoO_4)_7$, measured at a field strength of 100 G. The inset shows the inverse magnetization for the field-cooled (FC) mode together with a modified Curie–Weiss fit as straight line. (b) Field dependence of magnetization of $CsFe_5(MoO_4)_7$, measured at 2 K. Magnetic hysteresis loops at 2 K show stepwise increases in magnetization with field.

which is estimated based on the spin contribution of two Fe^{2+} and three Fe^{3+} ions.

Neutron Diffraction Study

The refinement of neutron powder diffraction data of a $CsFe_5(MoO_4)_7$ sample at 30 K revealed the presence of following phases: $CsFe_5(MoO_4)_7$ (ca. 90% w/w), nuclear and magnetic structures of α-$FeMoO_4$[14] (1% w/w) and α-Fe_2O_3 (2% w/w), and $CsFe(MoO_4)_2$[9] (7% w/w) (see Figure 12).

Cooling from 30 to 4 K resulted in the appearance of several superstructural reflections of magnetic origin. These additional reflections cannot be due to the presence of α-$FeMoO_4$, which has an antiferromagnetic ordering temperature of 35 K,[14] or hematite α-Fe_2O_3 with a Morin transition temperature below 260 K and a very much higher magnetic ordering temperature.

The majority of superstructural reflections can be indexed by assuming the magnetic cell doubling in the *a* direction with propagation vector $\mathbf{k} = (^1/_2,0,0)$. The possible magnetic structures compatible with the symmetry of $CsFe_5(MoO_4)_7$ are determined by the representation analysis technique described by Bertaut.[15] For the propagation

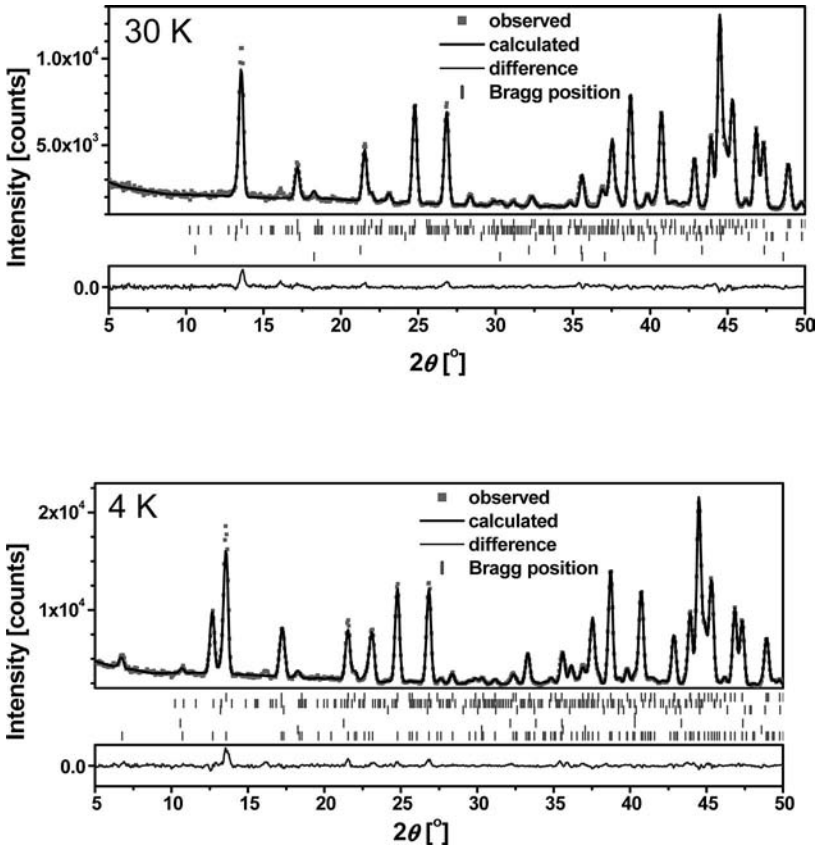

Figure 12. Low-angle section of the neutron diffraction patterns from $CsFe_5(MoO_4)_7$ sample at 30 and 4 K, above and below the magnetic phase transition. The positions of the Bragg reflections at 30 K correspond from top to bottom to the crystal structure of $CsFe_5(MoO_4)_7$, and nuclear and magnetic structures of α-$FeMoO_4$ and α-Fe_2O_3. The positions of the magnetic Bragg reflections of $CsFe_5(MoO_4)_7$ at 4 K are shown by the lower line of marks in the bottom figure as corresponds to propagation vectors $\mathbf{k} = (^1/_2,0,0)$ and $\mathbf{k} = (0,0,0)$.

Table 4. Irreducible representations and basis vectors for the magnetic moments on the Fe sites in $CsFe_5(MoO_4)_7$ [space group $P2_1/m$, for $\mathbf{k}_{12} = (^1/_2,0,0)$]. The symmetry elements are written according to Kovalev's notation.[16]

	$\{h_1\|0,0,0\}$				$\{h_4\|0,^1/_2,0\}$				$\{h_{25}\|0,0,0\}$				$\{h_{28}\|0,-^1/_2,0\}$			
Γ_1	1				1				1				1			
Γ_2	1				1				−1				−1			
Γ_3	1				−1				1				−1			
Γ_4	1				−1				−1				1			
	Fe_1(0.34907(52),0.10021(13),0.33937(35))				Fe_2(0.95319(67),¼,0.68698(49))				Fe_3(0.02864(51),0.50261(14),0.18751(33))							
	x,y,z	$-x+1,y+^1/_2,-z+1$	$-x+1,y+^1/_2,-z+1$	$x,-y+^1/_2,z$	x,y,z	$-x+1,y+^1/_2,-z+1$			x,y,z	$-x+1,y+^1/_2,-z+1$	$-x+1,y-^1/_2,-z+1$	$x,-y+^3/_2,z$				
Γ_1	u,v,w	$u,-v,w$	$-u,-v,-w$	$-u,v,-w$	$0,v,0$	$0,-v,0$			u,v,w	$u,-v,w$	$-u,-v,-w$	$-u,v,-w$				
Γ_2	u,v,w	$u,-v,w$	u,v,w	$u,-v,w$	$u,0,w$	$u,0,w$			u,v,w	$u,-v,w$	u,v,w	$u,-v,w$				
Γ_3	u,v,w	$-u,v,-w$	$-u,-v,-w$	$u,-v,w$	$u,0,w$	$-u,0,-w$			u,v,w	$-u,v,-w$	$-u,-v,-w$	$u,-v,w$				
Γ_4	u,v,w	$-u,v,-w$	u,v,w	$-u,v,-w$	$0,v,0$	$0,v,0$			u,v,w	$-u,v,-w$	u,v,w	$-u,v,-w$				

vector **k** = ($^1/_2$,0,0), the small group $\mathbf{G}_k$, formed by those elements of the space group that leave **k** invariant, coincides with the space group $P2_1/m$. For **k** = ($^1/_2$,0,0), the irreducible representations of the group $\mathbf{G}_k$ are shown in Table 4.

A representation is constructed with the Fourier components $\mathbf{m}_k$ that correspond to the Fe atoms in $CsFe_5(MoO_4)_7$, and the decomposition of the representation in terms of the irreducible representations Γ_k for each Fe site reads as follows: $\Gamma(Fe_1) = 3\Gamma_1^1 + 3\Gamma_2^1 + 3\Gamma_3^1 + 3\Gamma_4^1$; $\Gamma(Fe_2) = 1\Gamma_1^1 + 2\Gamma_2^1 + 2\Gamma_3^1 + 1\Gamma_4^1$; $\Gamma(Fe_3) = 3\Gamma_1^1 + 3\Gamma_2^1 + 3\Gamma_3^1 + 3\Gamma_4^1$. The different basis vectors that correspond to each irreducible representation were calculated by using the projection operator technique implemented in SARAh[17] and are listed in Table 4. Four possible configurations of magnetic ordering (those corresponding to $\Gamma_{1.4}$ representations) were tested, and the best agreement has been obtained for Γ_1.

Nevertheless, this model cannot serve as an adequate description of magnetic ordering in $CsFe_5(MoO_4)_7$ as it was unable to simulate the first observed magnetic reflection at 6.79°, which can only be satisfactorily described as 010 [i.e., **k** = (0,0,0)]. Furthermore, a nearly zero magnetic moment was deduced on the Fe(2) (2*e* site). Different possible magnetic arrangements have been tested on the basis of such a multi-k structure with **k** = ($^1/_2$,0,0) for Fe(1) and Fe(3) and **k** = (0,0,0) for Fe(2). The best agreement (R_{mag} = 7.20%) has been found for a magnetic structure with magnetic moments μ[Fe(1)] = [1.7(1),0.0,2.35(6)] μ_B, $|\mu[Fe(1)]| \approx 2.6\ \mu_B$; μ[Fe(2)] = [0.0,0.0,1.6(2)] μ_B; μ[Fe(3)] = [0.0,0.8(1), 3.38(4)] μ_B, $|\mu[Fe(3)]| \approx 3.5\ \mu_B$. This magnetic structure model for $CsFe_5(MoO_4)_7$ is shown for different projections in Figure 13, and is discussed with respect to the underlying exchange couplings.

The most important superexchange and supersuperexchange couplings are summarized in Table 5. There is no obvious and simple rule for the resulting magnetic arrangement in terms of the geometry of the coupling paths. Nevertheless, a peculiarity of the Fe(2) site is revealed. It seems that magnetic moments on the Fe(2) site are not only smaller than for the other Fe sites, but also favour ferromagnetic couplings instead of antiferromagnetic ones. However, the crystal and magnetic structures of $CsFe_5(MoO_4)_7$ are too complicated to draw unambiguous conclusions about the underlying interactions, especially in

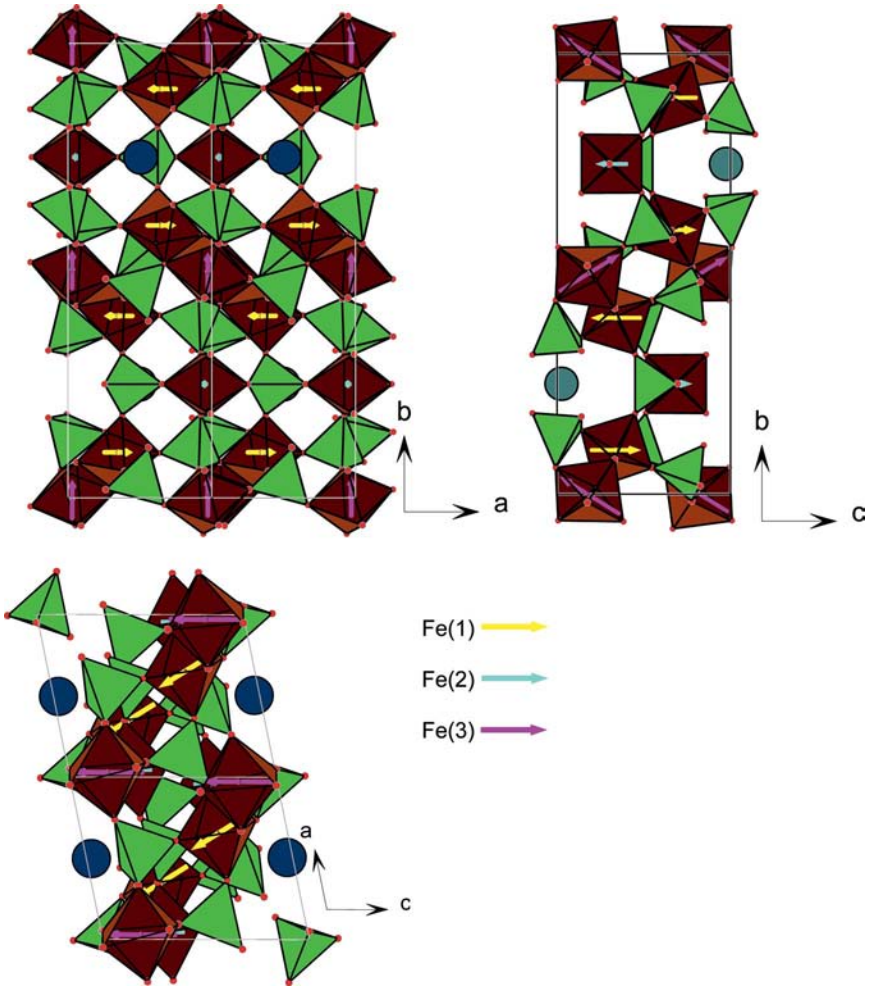

Figure 13. Magnetic structure of $CsFe_5(MoO_4)_7$ in different crystallographic planes. The orientation of Fe magnetic moments are shown by arrows. Fe(1)–(3) correspond to atomic coordinates from Table 2.

Table 5. Superexchange (top) and supersuperexchange (bottom) paths based on the structural parameters from low-temperature (4 K) neutron diffraction. Only unique supersuperexchange paths with sufficiently large Fe–O–O and O–O–Fe angles that correspond to Fe–Fe distances above 6 Å are listed. Note that parallel (F) or antiparallel (AF) arrangement refers to the dominant magnetic components along the *c* axis only.

	F/AF	Geometry of the Fe–O–Fe superexchange path, bond lengths in Å							*d* [Å]
J_A	↑↓	Fe(1)	– 2.043	100.76° O(24)[–100]	– 2.126			Fe(3)	3.211
			– 2.058	101.73° O(41)	– 2.083				
J_B	↑↑	Fe(3)	– 2.141	100.04° O(13)	– 2.019			Fe(3)[–10–1]	3.188
	F/AF	Geometry of Fe–O–O–Fe supersuperexchange paths, bond lengths in Å							*d* [Å]
J_1	↑↑	Fe(2)	– 2.036	154.60° O(22)	Mo(2) 3.018	156.08° O(24)	– 2.126	Fe(3)[100]	7.007
J_2	↑↓	Fe(1)	– 1.982	172.62° O(21)	Mo(2) 2.978	158.49° O(24)	– 2.043	Fe(1)[100]	6.918
J_3	↑↑	Fe(2)	– 2.058	174.21° O(32)[100]	Mo(3)[100] 2.835	174.49° O(31)[100]	– 2.033	Fe(2)[100]	6.918
J_4	↑↓	Fe(3)	– 2.083	150.07° O(41)	Mo(4) 3.031	153.71° O(42)	– 2.017	Fe(3)[100]	6.918
J_5	↑↑	Fe(2)	– 2.033	155.67° O(12)[101]	Mo(1)[101] 2.924	148.15° O(13)[101]	– 2.141	Fe(3)[101]	6.881
J_6	↑↓	Fe(1)	– 1.961	156.04° O(11)	Mo(1) 2.878	141.61° O(12)	– 2.033	Fe(2)[–10–1]	6.587
J_7	↑↓	Fe(1)	– 1.986	152.28° O(33)	Mo(3) 2.900	152.28° O(33)	– 1.986	Fe(1)	6.416

light of the canted magnetic moments, which reflect additional Dzyaloshinskii–Moriya-type interactions besides the Heisenberg super- and supersuperexchanges.

Conclusion

In the present work, average interatomic Mo–O distances in all investigated Cs,Fe molybdates (1.74–1.76 Å) correspond to the one in Li_2MoO_4 (1.764 Å,[18]) and point out the presence of only molybdenum(VI). For $CsFe_5(MoO_4)_7$ with $Fe^{+2.6}$, there are three different Fe sites in the structure: two 4*f* and one 2*e*. Based on charge neutrality, a simple ionic model of localized electrons would suggest the existence of Fe^{3+} on one 4*f* and the 2*e* site and Fe^{2+} on the other 4*f* site. Analysis of Fe–O bond lengths in FeO_6 octahedra showed the shortest [2.01(5) Å] and the longest Fe–O [2.08(5) Å] average distances for both Fe on 4*f* sites. They form Fe_4O_{18} units with Fe–Fe distances of about 3.2 Å, which together with strong octahedral distortion of FeO_6 allow us to conclude rather a delocalized character of electrons. Determination of the antiferromagnetic structure of $CsFe_5(MoO_4)_7$ from neutron powder diffraction revealed the smallest magnetic moment of 1.6 μ_B for Fe on the 2*e* site in comparison to 2.6 and 3.5 μ_B for Fe on 4*f* sites.

Complex molybdates of an alkaline metal and Fe^{II} with Mo_yO_x clusters and a metallic Mo–Mo bond seem to be stable only for a small alkaline element. All attempts to obtain Cs,Fe molybdates with Fe^{2+} and Mo in an oxidation state lower than +6, for example, in $Na_3Fe_2Mo_5O_{16}$ with metallic Mo–Mo bonds,[19] led to the formation of different Mo oxides, metallic molybdenum, Fe oxides and Cs_2MoO_4.

Experimental Section

Sample Preparation: The initial reactants used for syntheses were $CsNO_3$, Fe_2O_3, FeO, MoO_3 (Alfa Aesar) with a degree of purity > 99.99% (metal basis). The intermediate product caesium molybdate, Cs_2MoO_4, was prepared by solid-state reaction from caesium nitrate and molybdenum oxide with a first step under argon at 623 K for 20 h, followed by a second step in air with increasing temperature stepwise by 50 K and a hold time of 10–12 h at each temperature. The final synthesis temperature was 1023 K. Single crystals of $Cs_2Fe_2(MoO_4)_3$, $Cs_4Fe(MoO_4)_3$ and $CsFe_5(MoO_4)_7$ were grown from mixtures of Cs_2MoO_4, Fe_2O_3, FeO and MoO_3 according to the following chemical reactions by the flux method [Equations (1), (2) and (3)]:

$$Cs_2MoO_4 + 2\ FeO + 2\ MoO_3 \rightarrow Cs_2Fe_2(MoO_4)_3 \quad (1)$$

$$2\ Cs_2MoO_4 + FeO + MoO_3 \rightarrow Cs_4Fe(MoO_4)_3 \quad (2)$$

$$Cs_2MoO_4 + 4\ FeO + 3\ Fe_2O_3 + 13\ MoO_3 \rightarrow 2\ CsFe_5(MoO_4)_7 \quad (3)$$

Starting components with a total mass of 1 g were weighed with an accuracy of 0.00005 g and ground in a mortar. The mixture was put into a silica tube, which was evacuated and sealed under vacuum (10^{-4} mbar). The tube was heated up to 823–1023 K, kept at this temperature for 20–30 h and then cooled to room temperature. The final synthesis temperature for $Cs_2Fe_2(MoO_4)_3$ and $CsFe_5(MoO_4)_7$ compositions was 1023 K (30 h), for $CsFe_4(MoO_4)_3$ 823 K (20 h). Polycrystalline samples $CsFe_5(MoO_4)_7$ were synthesized under a dynamic vacuum at 973 K according to Equation (3).

Single-Crystal Diffraction: Single-crystal X-ray diffraction data for all compounds – $Cs_2Fe_2(MoO_4)_3$, $Cs_4Fe(MoO_4)_3$ and $CsFe_5(MoO_4)_7$ – were collected by using graphite-monochromatized Mo-

Table 6. Crystal data and structure refinement.

Empirical formula	$Cs_2Fe_2(MoO_4)_3$	$CsFe_5(MoO_4)_7$	$Cs_4Fe(MoO_4)_3$
M_r	857.34	1531.74	1067.31
Crystal system	cubic	monoclinic	trigonal
Space group	$P2_13$	$P2_1/m$	$P\bar{6}2c$
a [Å] at 298 K	10.9161(2)	6.9239(6)	6.2922(16)
b [Å] at 298 K		21.4477(19)	
c [Å] at 298 K		8.6374(8)	23.937(13)
β [°] at 298 K		101.667(2)	
V [Å^3]	1300.78(4)	1256.17(19)	820.7(5)
a [Å] at 100 K	10.8910(4)	6.9171(4)	6.2529(8)
b [Å] at 100 K		21.4097(11)	
c [Å] at 100 K		8.6384(5)	23.9368(15)
β [°] at 100 K		101.641(1)	
V [Å^3]	1291.82(8)	1252.97(1)	810.51(6)
Z	4	2	2
$\rho_{calcd.}$ [g cm^{-3}]	4.378	4.050	4.319
Absorption coefficient [mm^{-1}]	10.557	7.696	11.892
$F(000)$	1536	1406	936
Crystal size [mm]	$0.07 \times 0.05 \times 0.04$	$0.06 \times 0.04 \times 0.04$	$0.14 \times 0.10 \times 0.06$
θ range for data collection [°]	2.64–32.87	1.90–30.51	1.70–30.59
Index ranges	$-16 \le h \le 7$	$-9 \le h \le 4$	$-8 \le h \le 8$
	$-16 \le k \le 14$	$-25 \le k \le 30$	$-8 \le k \le 5$
	$-16 \le l \le 15$	$-11 \le l \le 12$	$-34 \le l \le 28$
Reflections collected	10034	9053	3980
Independent reflections	1562 [R(int) = 0.0279]	3904 [R(int) = 0.0205]	805 [R(int) = 0.0313]
Completeness to θ = 25.00° [%]	100.0	99.8	98.5
Max./min. transmission	0.6775/0.5253	0.7483/0.6552	0.5356/0.2868
Data/restraints/parameters	1562/0/60	3904/0/194	805/0/39
Goodness-of-fit on F^2	1.433	1.028	1.035
Final R indices [$I > 2\sigma(I)$]	R_1 = 0.0129	R_1 = 0.0212	R_1 = 0.0175
	wR_2 = 0.0294	wR_2 = 0.0485	wR_2 = 0.0367
R indices (all data)	R_1 = 0.0141	R_1 = 0.0267	R_1 = 0.0267
	wR_2 = 0.0296	wR_2 = 0.0497	wR_2 = 0.0394
Absolute structure parameter	0.001(12)		0.38(7)
Extinction coefficient	0.00270(13)	0.00046(8)	0.00338(15)
Largest diff. peak/hole [e Å^{-3}]	0.763/–0.496	2.643/–1.269	0.551/–0.365

K_α radiation (λ = 0.71073 Å) at 298(2) and 100(2) K with a Bruker Kappa Apex II CCD diffractometer equipped with a 4 k CCD area detector (Table 6). The ϕ-scan technique was employed to measure intensities. Absorption corrections were applied by using the SADABS program.[20] The crystal structures were solved by direct methods and were refined by full-matrix least-squares techniques with the use of the SHELXTL package.[21] All atomic thermal parameters were refined anisotropically. Since single-crystal X-ray diffraction experiments at 298 and 100 K revealed no phase transition in this temperature range, only cell parameters at 100 K are given in Table 6, whereas all further structure descriptions and refined parameters are based on the room-temperature experiments. Further details of the crystal structure investigations can be obtained from the Fachinformationszentrum Karlsruhe, 76344 Eggenstein-Leopoldshafen, Germany (Fax: +49-7247-808-666; E-mail: crysdata@fiz-karlsruhe.de, http://www.fiz-karlsruhe.de/request_for_deposited_data.html) on quoting the depository numbers CSD-422752 [for $Cs_2Fe_2(MoO_4)_3$], -422753 [for $Cs_4Fe(MoO_4)_3$], and -422754 [for $CsFe_5(MoO_4)_7$].

Powder X-ray Diffraction: Phase analysis and determination of cell parameters at room temperature of $CsFe_5(MoO_4)_7$ were carried out by means of X-ray powder diffraction (XPD) with a STOE STADI P diffractometer (Cu-$K_{\alpha1}$ radiation, λ = 1.54059 Å) in transmission mode and by applying Rietveld refinements using FULLPROF.

Powder Neutron Diffraction: Elastic coherent neutron scattering experiments were performed on the high-resolution powder diffractometer SPODI at the research reactor FRM-II (Garching, Germany) with monochromatic neutrons of 1.5481(1) Å wavelength.[22] Measurements were performed in Debye–Scherrer geometry. The powder sample (ca. 0.3 cm^3 in volume) was filled into a thin-wall (0.15 mm) vanadium can (10 mm in diameter) and then mounted in the top-loading closed-cycle refrigerator. Helium 4 was used as a heat transmitter. The instantaneous temperature was measured with two thin-film resistance cryogenic temperature sensors Cernox and controlled by a temperature controller from LakeShore. Two-dimensional powder diffraction data were collected at 4 and 30 K by using a wavelength of 2.536 Å, and then corrected for geometrical aberrations and curvature of Debye–Scherrer rings.

Magnetic Properties: The magnetic properties of $CsFe_5(MoO_4)_7$ were studied with a superconducting quantum interference device (SQUID) from Quantum Design. The sample was placed inside a gelatine capsule and fixed inside a straw attached to the rod, which is part of the SQUID device and enables the positioning and controlled movement of the sample. The measurements were performed under helium. Measurements were performed upon heating in field-cooled (FC) and zero-field-cooled (ZFC) mode in the temperature range from 1.8 to 350 K and a field strength of up to 6.0 T.

Acknowledgments

This work was financially supported by the Bundesministerium für Bildung und Forschung, Germany (grant no. 03FU7DAR).

[1] J. A. Ibers, G. W. Smith, *Acta Crystallogr.* **1964**, *17*, 190–197.
[2] M. V. Mokhosoev, F. P. Alekseev, V. L. Butukhanov, *Double Molybdates and Tungstates*, Nauka, Novosibirsk, **1981**.
[3] A. Sarapulova, D. Mikhailova, A. Senyshyn, H. Ehrenberg, *J. Solid State Chem.* **2009**, *182*, 3262–3268.
[4] D. Mikhailova, A. Sarapulova, A. Voss, A. Thomas, S. Oswald, W. Gruner, D. M. Trots, N. N. Bramnik, H. Ehrenberg, *Chem. Mater.* **2010**, *22*, 3165–3173.
[5] C. Gicquel-Mayer, G. Perez, *Rev. Chim. Miner.* **1975**, *12*, 537–545.
[6] J. M. Engel, H. Ahsbahs, H. Fuess, H. Ehrenberg, *Acta Crystallogr., Sect. B* **2009**, *65*, 29–35.
[7] E. Muessig, K. G. Bramnik, H. Ehrenberg, *Acta Crystallogr., Sect. B* **2003**, *59*, 611–616.
[8] L. Balsanova, D. Mikhailova, A. Senyshyn, D. Trots, H. Fuess, W. Lottermoser, H. Ehrenberg, *Solid State Sci.* **2009**, *11*, 1137–1143.
[9] B. G. Bazarov, T. V. Namsaraeva, R. F. Klevtsova, K. N. Fedorov, L. A. Glinskaja, Z. G. Bazarova, *Kristallografiya* **2010**, *55*, 633–635.
[10] K. M. Khal'baeva, S. F. Solodovnikov, E. G. Khaikina, Y. M. Kadyrova, Z. A. Solodovnikova, O. M. Basovich, *J. Solid State Chem.* **2010**, *183*, 712–719.
[11] S. F. Solodovnikov, R. F. Klevtsova, V. G. Kim, P. V. Klevtsov, *Zh. Strukt. Khim.* **1986**, *27*, 928–933.
[12] *Inorganic Crystal Structure Database (ICSD)* **2010**-1, Fachinformationszentrum Karlsruhe, Germany.
[13] S. F. Solodovnikov, R. F. Klevtsova, L. A. Glinskaya, P. V. Klevtsov, *Kristallografiya* **1988**, *33*, 1380–1386.
[14] H. Ehrenberg, G. Wltschek, F. Trouw, T. Kroener, H. Weitzel, H. Fuess, *J. Magn. Magn. Mater.* **1994**, *135*, 355–360.
[15] E. F. Bertaut, *Acta Crystallogr., Sect. A* **1968**, *24*, 217–231.
[16] O. V. Kovalev, in *Representations of the Crystallographic Space Groups: Irreducible Representations, Induced Representations and Corepresentations* (Eds.: H. T. Stokes, D. M. Hatch), Gordon and Breach, Amsterdam, **1993**.
[17] A. S. Wills, *Phys. B* **2000**, *276*, 680–681.
[18] U. Kolitsch, *Z. Kristallogr.* **2001**, *216*, 449–454.
[19] K. G. Bramnik, E. Muessig, H. Ehrenberg, *J. Solid State Chem.* **2003**, *176*, 192–197.
[20] Bruker AXS Inc., *APEX2* (Version 1.08), *SAINT* (Version 7.03) and *SADABS* (Version 2.11), Bruker Advanced X-ray Solutions, Madison, Wisconsin, USA, **2004**.
[21] G. M. Sheldrick, *Acta Crystallogr., Sect. A* **2008**, *64*, 112–122.
[22] M. Hoelzel, A. Senyshyn, R. Gilles, H. Boysen, H. Fuess, *Neutron News* **2008**, *18*, 23.

Received: January 18, 2011
Published Online: May 19, 2011

